Dielectric Characterization by Microwave Cavity Perturbation Corrected for Nonuniform Fields

Nathan D. Orloff, Jan Obrzut, Christian J. Long, Thomas Lam, Pavel Kabos, *Fellow, IEEE*, David R. Novotny, James C. Booth, and J. Alexander Liddle

***Abstract*—Nonuniform fields decrease the accuracy of dielectric characterization by microwave cavity perturbation. These fields are due to the slot in the cavity through which the sample is inserted and the boundary between the sample and the metallic walls inside of the cavity. To address this problem, we measured the natural frequency and damping ratio of a resonant cavity as a sample is inserted into the rectangular cavity. We found that for a range of cavity filling fractions, a linear regression on the natural frequency and damping ratio versus the effective volume fraction of the sample in the cavity could be used to extract the complex permittivity of the sample. We verified our technique by measuring a known quartz substrate and comparing the results to finite-element simulations. When compared to the conventional technique, we found a significant improvement in the accuracy for our samples and measurement setup. We confirmed our technique on two lossy samples: a neat stoichiometric mixture bisphenol A epoxy resin and one containing a mass fraction of 3.5% multi-walled carbon nanotubes (MWCNTs). At the TE_{103} mode (7.31 GHz), the permittivity and loss tangent of the epoxy were measured to be $\epsilon_r = 2.93 \pm 0.11$ and $\tan\delta = 0.028 \pm 0.002$, respectively. The epoxy with a mass fraction of 3.5% MWCNTs had a permittivity of $\epsilon_r = 8.01 \pm 0.48$ and loss tangent of $\tan\delta = 0.137 \pm 0.010$.**

***Index Terms*—Bisphenol A epoxy, metrology, microwave, multi-walled carbon nanotubes (MWCNTs), nanocomposites, noncontact, nondestructive, resonator.**

I. Introduction

COMPLEX permittivity measurement by resonant cavity perturbation has been established in the literature for over 70 years [1]–[4]. Since its first demonstration [1], it has become a preferred technique for characterizing the complex permittivity of materials ($\tilde{\epsilon} = \epsilon_r - i\epsilon_i$) at microwave frequencies [5], [6]. Cavity perturbation is attractive as a means for quantifying the permittivity [7]–[11] because it is noncontact, nondestructive, and experimentally simple, in contrast to electrode-based techniques (e.g., [12] and [13]). Despite its popularity, this technique has many limitations [4]. If the sample is too large or has a permittivity or loss tangent ($\tan\delta = \epsilon_i/\epsilon_r$) that is too high, then the field distribution is significantly altered, making the perturbation approach inaccurate [14]. Furthermore, the depolarization fields in the sample decrease the resonance frequency shift, implying that there will be a discrepancy between the measured and actual sample permittivity [8], [15]. This discrepancy is dependent on the complex permittivity of the sample, the sample geometry, the geometry of the cavity, and even the geometry of the slot through which a sample is inserted into the cavity.

One possible solution to resolving the contribution of the nonuniform fields is to partially insert the sample into the cavity [8], [16], [17]. In this case, there is always some filling fraction where the fields are approximately uniform over a region in the sample. Unfortunately, this gives rise to a large nonuniform depolarization field at the boundary between the sample and the cavity. Previous reports on cavity perturbation with partial filling found that this factor was not negligible, and rendered the analytical expressions used to obtain complex permittivity inaccurate at low partial fillings fractions [8], [16]. Here, we present an approach to correct for the nonuniform fields in the sample, which improves the accuracy of this technique and offers an explanation for the inaccuracy. Our technique has the potential to permit the measurement of strongly perturbing [17] and small samples that would not be possible with the conventional approach or alternatives (e.g., the split-cylinder technique [18], [19]).

In what follows, we demonstrate that the resonances can be fit with a damped harmonic oscillator model (Section III-B), which is then used to the extract the natural frequency and damping ratio. We show that the relative natural frequency and sample damping ratio are linearly dependent on the effective volume fraction (Section III-C). We show that the slopes of the best fit lines are directly related to the complex permittivity (Section III-D). We validate our technique with a fused quartz substrate and a bisphenol A epoxy resin, and with finite-element simulations. We then compare two samples with similar dimensions, but different material properties [bisphenol A epoxy resin, and the same resin containing a mass fraction of 3.5% multi-walled carbon nanotubes (MWCNTs)] to better understand the role of dielectric loss (Section IV).

Manuscript received February 03, 2014; revised May 20, 2014; accepted June 13, 2014. Date of publication July 23, 2014; date of current version September 02, 2014.

N. D. Orloff, J. Obrzut, C. J. Long, T. Lam, and J. A. Liddle are with the National Institute of Standards and Technology (NIST), Gaithersburg, MD 20906 USA (e-mail: orloff@nist.gov; jan.obrzut@nist.gov).

P. Kabos, D. R. Novotny, and J. C. Booth, are with the National Institute of Standards and Technology (NIST), Boulder, CO 80305 USA.

Color versions of one or more of the figures in this paper are available online at http://ieeexplore.ieee.org.

Digital Object Identifier 10.1109/TMTT.2014.2336775

II. Theory

The classic perturbation equation derived directly from Maxwell's equations is

$$\frac{\Delta\tilde{\omega}}{\tilde{\omega}_c} = \frac{\int_{V_s}\left[(\bar{E}_s\cdot\bar{D}_c - \bar{E}_c\cdot\bar{D}_s) - (\bar{H}_s\cdot\bar{B}_c - \bar{H}_c\cdot\bar{B}_s)\right]dV}{\int_{V_c}(\bar{E}_c\cdot\bar{D}_c - \bar{H}_c\cdot\bar{B}_c)dV} \tag{1}$$

where $\Delta\tilde{\omega} = \tilde{\omega_{cs}} - \tilde{\omega_c}$ is the frequency shift between the complex resonance frequency of the cavity with the sample $(\tilde{\omega_{cs}})$ and the complex resonance frequency $(\tilde{\omega_c})$ of the cavity [4]. The complex resonance frequency $(\tilde{\omega})$ is approximated as $\tilde{\omega} \approx \omega_o + i\zeta$, where ω_o is the natural frequency and ζ is the damping ratio $(\zeta = 1/2Q)$ [6], [20]. In our case, the sample and the inside of the cavity are nonmagnetic, hence the terms with H and B in the numerator vanish. The volume integral over term $\bar{H}_c\cdot\bar{B}_c$ in the denominator is absorbed as a factor of 2 because the time average of the energy is twice the energy stored in the electric field [3]. We multiply both sides by negative one and rearrange (1) [6]. We then substitute the displacement field in the sample by $\bar{D}_s = \bar{D}_s^{uni} - \bar{D}_s^{\text{non}}$, where $\bar{D}_s^{uni}$ is the uniform field in the sample and $\bar{D}_s^{\text{non}}$ is the nonuniform field in the sample due to the depolarization field, the slot in the waveguide, and so on. The permittivity of the cavity without the sample is the permittivity of free space so (1) reduces to

$$\frac{\tilde{\omega_c} - \tilde{\omega_{cs}}}{\tilde{\omega_c}} \approx \frac{(\tilde{\epsilon}-1)\int_{V_s}|\bar{E}_c|^2dV - \int_{V_s}\left(\bar{E}_c\cdot\bar{D}_s^{\text{non}}\right)dV}{2\int_{V_c}|\bar{E}_c|^2dV}. \tag{2}$$

Since we performed our measurements in a rectangular cavity operating in the TE_{10n} mode (n was the mode number), we solved Maxwell's equations and wrote the analytical expression for the electric field in the cavity [21]. We chose a rectangular cavity because of our sample geometry. We then evaluate the volume integral in the numerator to define the effective sample volume as

$$V_s' = ht'w'. \tag{3}$$

The effective sample thickness t' and width w' are given by

$$t' = \left(\frac{t}{2} + \frac{d}{2\pi}\sin\left(\frac{\pi t}{d}\right)\right) \text{ and } w' = \left(\frac{w}{2} + \frac{\ell}{2\pi n}\sin\left(\frac{n\pi w}{\ell}\right)\right). \tag{4}$$

Here, w and t are the width and thickness of the sample and ℓ and d are the dimensions of the cavity [see Fig. 1(a) and (b)]. The sample is inserted into the cavity a length h. The filling fraction is h/a. Although shown previously [20], [22]–[24], we report effective sample thickness and width because it is relevant to the uncertainty analysis. We evaluate the volume integral over the field in the cavity as $|\bar{E}_o|^2V_c/4$, where V_c is the volume of the cavity and E_o is the maximum electric field. After following these steps, we find that (2) reduces to

$$\frac{\tilde{\omega_c} - \tilde{\omega_{cs}}}{\tilde{\omega_c}} \approx 2(\tilde{\epsilon}-1)\frac{V_s'}{V_c} - \frac{2\int_{V_s}\left(\bar{E}_c\cdot\bar{D}_s^{\text{non}}\right)dV}{|\bar{E}_o|^2V_c}. \tag{5}$$

For our purposes, we define three parameters,

$$x \equiv \frac{V_s'}{V_c} \quad y_r \equiv \frac{\omega_c - \omega_{cs}}{\omega_c} \quad y_i \equiv \frac{1}{Q_{cs}} - \frac{1}{Q_c} \tag{6}$$

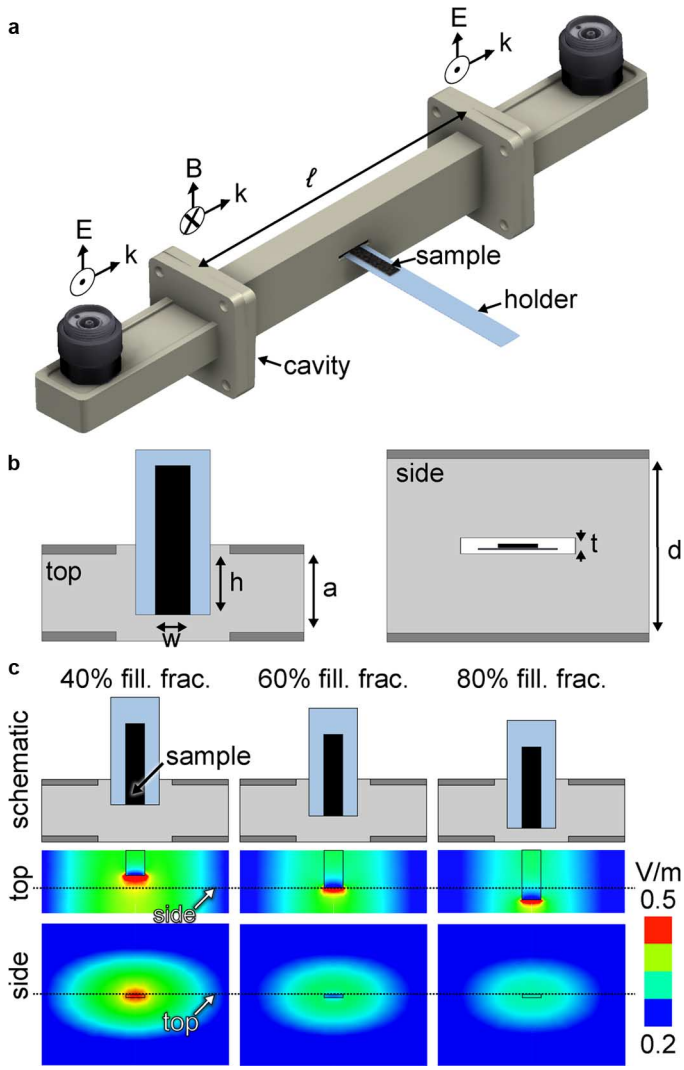

Fig. 1. Diagram of the partial filling measurement setup. (a) Cross-polarized cavity resonator. (b) Side view and top view of the sample in the cavity with the dimensions of the cavity (thickness d and height a). The sample dimensions are t, h, and w for thickness, height, and width, respectively. (c) Field structure as a function of filling fraction (h/a) calculated by high-frequency finite-element simulation in the sample configuration shown in (b) for the TE_{103} mode at approximately 7.31 GHz. The sample in (c) has dimensions $w = 3.0$ mm, and $t = 0.5$ mm. The sample has a complex permittivity of $\tilde{\epsilon} = 10 + i0$. The thin dashed black lines in (c) indicate the top and side bisections.

and a term to encapsulate the nonuniform fields in the sample,

$$b \equiv \frac{2\int_{V_s}\left(\bar{E}_c\cdot\bar{D}_s^{\text{non}}\right)dV}{|\bar{E}_o|^2V_c} = b_r + ib_i. \tag{7}$$

In (6), x is the relative volume fraction of the sample, y_r is the relative frequency shift, and y_i is the sample damping ratio. Throughout, the subscripts r and i indicate the real and imaginary parts, respectively. This enables us to rewrite (2) as

$$y_r = (\epsilon_r - 1)2x - b_r \tag{8}$$

$$y_i = (\epsilon_i)4x - 2b_i. \tag{9}$$

In contrast, the conventional technique solves for the complex permittivity as $\epsilon_r = y_r/2x + 1$ and $\epsilon_i = y_i/4x$, which is true only when $b = 0$. From our measurements, we did not find any range of insertions (h) where $b = 0$, but we did notice that there

was a regime of values for h where $b \approx$ constant. In this case, (8) and (9) reduced to the equations of a line, and the values b_r and b_i contributed as intercepts.

The intercepts b_r and b_i are the result of integrating over the nonuniform fields inside the sample. To illustrate this effect, we used finite-element simulations to calculate the fields in the cavity to show how the fields accumulate at the edge of the sample as it is inserted into the cavity. Before this, we validated our finite-element simulations by reproducing the frequency response of the complex scattering parameters (S-parameters) of the empty cavity to within a few decibels in the measured frequency range. In Fig. 1(c), the nonuniform field can be seen near the edges of the sample in the direction of the E-vector for a sample that was 3.0-mm wide and 0.5-mm thick with a real part of the permittivity of $\epsilon_r = 10$ and a loss tangent of $\tan\delta = 0$. The simulation was for the TE_{103} mode. We used the TE_{103} mode because the TE_{101} mode was obscured by the cutoff frequency for our cavity. Higher order modes were measured, but for clarity, we only discuss the TE_{103} mode. The nonuniform field decreases the displacement field inside the sample near the boundary between the sample and the cavity, which in practice means that the measured relative frequency shift and sample damping ratio were less than expected for a sample with a given complex permittivity. In the coming sections, we will show the effect of the nonuniform fields and how they cause the measured permittivity to deviate from the correct values (Figs. 4 and 5).

III. Methodology

A. Measurement Setup

First, we connected a vector network analyzer (VNA) by semirigid coaxial cables to a WR90 (X-band) rectangular cavity via waveguide to coaxial adapters [see Fig. 2(a)]. The inside dimensions of the rectangular cavity were $a = (22.86 \pm 0.02)$ mm, $d = (10.16 \pm 0.02)$ mm, and $\ell = (134.92 \pm 0.03)$ mm. Unless otherwise noted, all length uncertainties were one standard deviation. In Fig. 2(a), we show the rectangular cavity connected between the couplers such that the E-vectors in the waveguide and coupler regions were slightly offset from perpendicular ($87.75\hat{z}$), called cross-polarized waveguides. The slight offset provided roughly frequency-independent coupling (-27.0 ± 2.6) dB at each port. Cross-polarized waveguides (rather than apertures) were convenient to model with finite-element simulations. For our measurements, we assumed that the port coupling $(\kappa = 0.06 \pm 0.01)$ was independent of the presence of the sample. The cavity had a slot (20.00 ± 0.03) mm wide by (1.50 ± 0.03) mm thick cut into the center, which allowed a sample on a holder to be inserted into the cavity. The slot was configured to not interfere significantly with the currents along the waveguide walls, reducing the effect of the slot on the fields inside the cavity. The sample (black) and holder (light blue in online version) are shown in Fig. 1(b). We used a (0.15 ± 0.02) mm thick glass sample holder that was (10.00 ± 0.02) mm wide and had a (0.05 ± 0.02) mm thick layer of polydimethylsiloxane (PDMS) spun onto the surface to hold the samples in place during the measurement [see Fig. 2(b)]. In Fig. 1(b), we show the sample dimensions

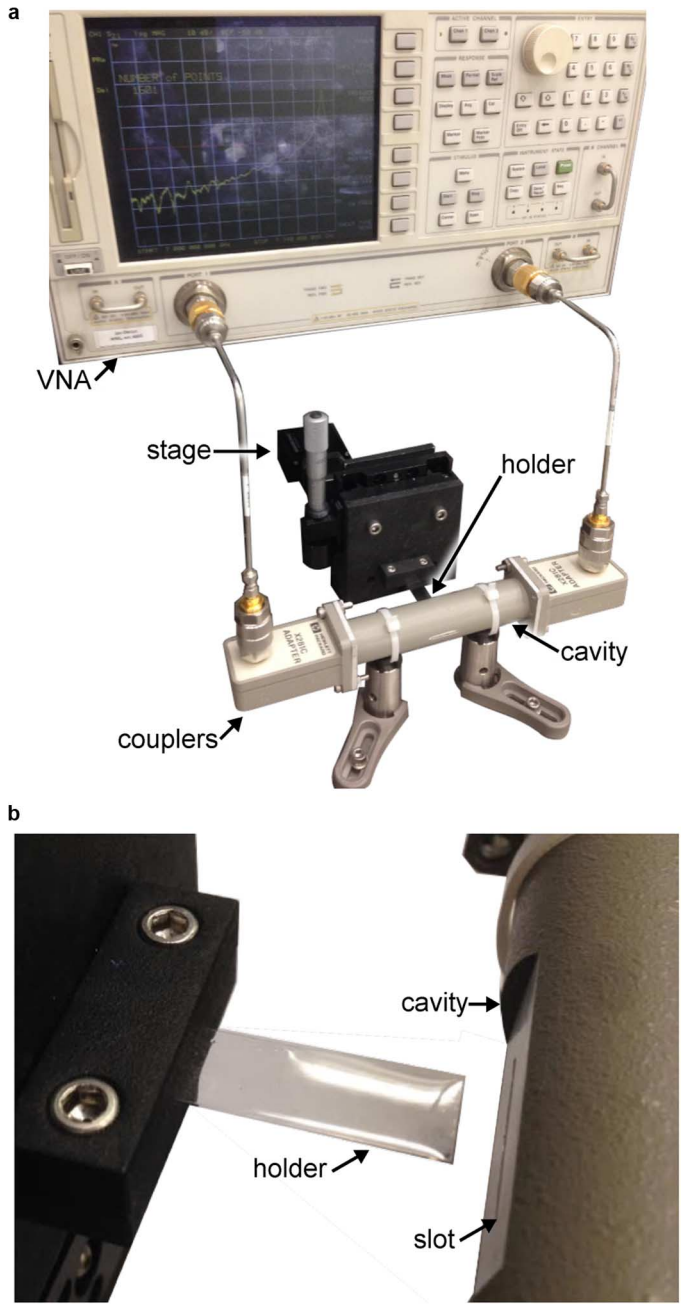

Fig. 2. (a) Photograph of the measurement setup. A motorized stage moves a sample on the sample holder into the cavity. (b) Close-up of the sample holder, slot, and cavity.

relative to the cavity. We varied h (the sample insertion) by an optically encoded linear stage controlled by a computer.

Our microwave measurements were performed from 7.1 to 7.45 GHz with 1601 frequency points at a power of -10 dBm and 300-Hz IF bandwidth. We measured the frequency-dependent S-parameters with each sample at $h = \{0.26\ \text{mm}, 0.51\ \text{mm}, 0.75\ \text{mm}, 1.00\ \text{mm}$ and, $2.00\ \text{mm}$ through 10.00 mm in 0.50 mm steps$\}$. We measured the cavity without the sample, which we called zero. The uncertainty on h was ± 0.02 mm. We measured 10.16 mm, which corresponds to 100% filling fraction. We measured four samples: the glass/PDMS sample holder, a 0.50-mm-thick quartz substrate,

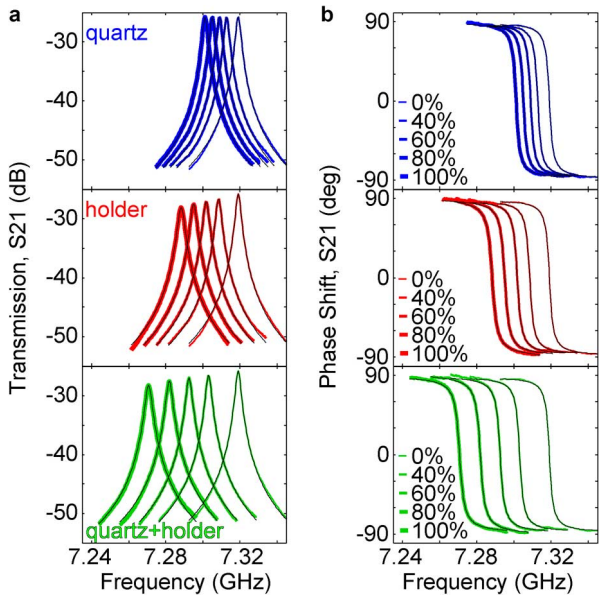

Fig. 3. Measurements of the amplitude and phase of the transmission coefficient (S_{21}) as a function of frequency for the quartz sample (blue in online version), the holder (red in online version), and the quartz sample on the holder (green in online version) for the TE_{103} mode at approximately 7.31 GHz. The black solid lines are the least squares fit to a damped harmonic oscillator model. (b) Phase shift due to the $\arctan$ term.

a 0.30-mm-thick epoxy substrate, and a 0.28-mm-thick epoxy composite with a mass fraction of a 3.5% MWCNT. Examples of the magnitude and phase of the transmission are shown in Fig. 3. See Section III-E for a step-by-step summary of the procedure.

B. Analysis

Having measured the complex S-parameters as a function of frequency for the various samples and filling fractions, we separated them into the real and imaginary parts of the transmission coefficients (S_{21}, S_{12}). The complex transmission coefficients were then modeled as a damped driven harmonic oscillator [25]–[27]. Fitting enabled us to more accurately obtain the loaded damping ratio for tested materials and the empty cavity [25]–[27], which is essential to the accuracy of cavity perturbation technique. In this case, the complex transmission $(S_{21,12} = A(\omega)e^{i\phi(\omega)})$ can be decomposed into a real amplitude

$$A(\omega) = \frac{2A_o\zeta_L\omega_o^2}{\left(\omega_o^2 - \omega^2\right)^2 + (2\zeta_L\omega_o\omega)^2} \tag{10}$$

and phase

$$\phi(\omega) = -\arctan\left(\frac{2\zeta_L\omega_o\omega}{\omega_o^2 - \omega^2}\right) + m_o\omega + \phi_o. \tag{11}$$

We fit the amplitude and phase as a function of frequency by a trust-region-reflective algorithm [28], weighting the frequency-dependent residuals by the amplitude of the resonance. This yielded three fit parameters: ω_o, the natural resonance frequency; A_o, approximately the amplitude of the transmission at resonance; ζ_L, the loaded damping ratio of the resonator. The remaining two parameters, m_o and ϕ_o, are the electrical delay and phase offset because the measurements were uncorrected by microwave calibration. In other instrumentation setups, it may be necessary to correct the measurements with calibration standards. Instead, we manually corrected for the delay due the cables [25]; hence, m_o and ϕ_o were close to zero. From this model, ω_o and ζ_L were the fit parameters used to map to the complex permittivity.

Next, we computed the fit parameter uncertainty by error propagation and used this to generate a 95% confidence interval on the fit parameters. In Fig. 3(a), we show the transmission in decibels as a function of frequency for four different filling fraction cases (40%, 60%, 80%, and 100%) for the quartz sample (blue in online version), the holder (red in online version), and the quartz sample on the holder (green in online version). The solid thin black lines that run through the middle of the data curves were the fit results obtained with (10) and (11). We show the phase for the different samples and filling fractions in Fig. 3(b). We tested a simplified version of our technique in Appendix A. We corrected the quality factors (and damping ratios) for the port coupling coefficient [29]–[31], but we neglected the correction to the natural frequency because it was several orders of magnitude smaller than the uncertainty.

C. Data Correction

Since we have a sample seated on a holder, it was essential to develop a correction procedure to isolate the contribution of the sample from that of the holder. In the following correction scheme, we isolated the perturbation due to the sample by taking three measurements: the empty cavity, the holder, and the sample on the holder. We required a sample holder for our measurements because the samples were physically smaller than the outside dimensions of the cavity. Hence, they required some support structure to allow them into be inserted to the cavity. It was reasonable to assume that the inductance of the cavity at resonance was unperturbed even if the sample had a small nonzero magnetic susceptibility provided the following conditions were met. First, the sample had to be placed inside the cavity symmetrically about an electric field maximum, which minimized the magnetic field density. In our case, we chose odd "n" cavity modes and placed the sample in the center of cavity. Second, the sample width (w) had to be much less than the guided wavelength, which reduced the contribution of fringing fields. In our procedure, we modeled a single resonance frequency as an equivalent lumped-element circuit, where the natural frequency was given by $\omega_o^{-2} = LC$ [6], [24]. Since the sample orientation was in the direction of the electric field, we modeled the contribution of the holder and sample as parallel admittances [5], [6], [24]. We used electronic design automation software to verify this treatment (Appendix B).

From this model, we can compute the natural frequency and quality factor of the cavity with the sample corrected for the effects of the holder [24]. In this case, the natural frequency of the cavity with the sample was given by

$$\omega_{cs}^{-2} \approx \omega_{chs}^{-2} - \omega_{ch}^{-2} + \omega_c^{-2}. \tag{12}$$

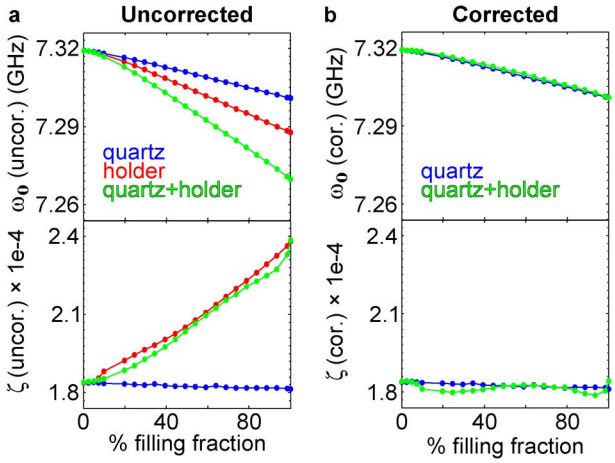

Fig. 4. Measurements of the natural frequency and damping ratio as a function of percent filling fraction for the uncorrected and corrected data of the quartz sample with and without the sample holder for the TE_{103} mode at approximately 7.31 GHz. The error bars are not shown because they are smaller than the plotted symbols.

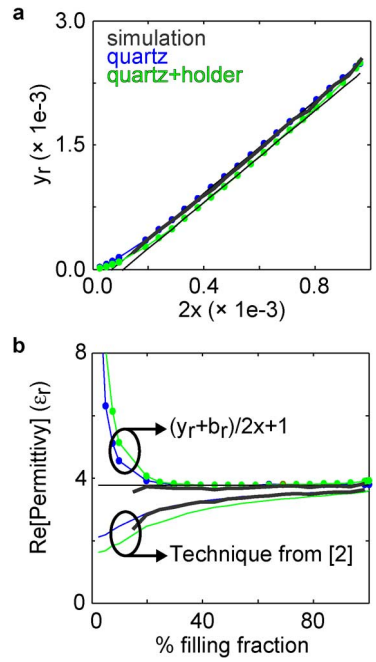

Fig. 5. Measurements and simulations of the relative frequency shift (y_r) versus the effective volume fraction (x) for our samples and measurement setup. In (b), we show the relative permittivity as a function of percent filling fraction for the TE_{103} mode at approximated 7.31 GHz. For both parts, we show the results for the sample-holder-corrected quartz (green in online version), the quartz sample measured without the sample holder (blue in online version), and simulations of the quartz sample without the sample holder (gray). Both the blue and green data were taken on the same quartz sample.

Likewise, the quality factor of the cavity with the sample can be solved for as

$$Q_{cs}^{-1} \approx Q_{chs}^{-1} - Q_{ch}^{-1} + Q_{c}^{-1}. \tag{13}$$

In both (12) and (13), the subscripts c, ch, and chs indicate measured parameters from the cavity, the cavity with the holder, and the cavity with the sample on the holder, respectively (Appendix C). From (12) and (13), we computed the corrected frequency shift for each sample at each filling fraction. Equations (12) and (13) are approximate because the port coupling might be dependent on the sample insertion. In our case, the correction factors were many orders of magnitude less than their respective uncertainties. In Fig. 4, we show the uncorrected (a) and corrected (b) natural frequency and damping ratio for the quartz sample as a function of effective volume fraction. Fig. 4(b) shows that following this correction scheme we were able to use measurements of the holder and the sample on the holder to recover the cavity perturbation due to the sample alone.

D. Validation

After correcting for the effect of the holder, we then determined the slopes from (8) and (9). In Fig. 5(a), we show the corrected relative frequency shift (y_r) versus the effective volume fraction (x) times two [see (8)] for the quartz sample on the holder (green in online version), quartz (blue in online version), and simulation (gray). The thin solid black lines were equations of best fit obtained by taking into account the uncertainties [32]. The material properties of the sample in the simulation were $\epsilon_r = 3.78$ and $\tan\delta = 0.001$ [33]–[36]. We solved for the cavity eigenmodes to obtain ω_o and ζ. To expedite the simulations, we placed a perfect magnetic boundary condition bisecting the cavity such that there was only a single port. We then varied the height (h) of the sample for each simulation. The linear regression of the simulated relative frequency shift versus effective volume fraction yielded $\epsilon_r = 3.76$. We remark that the data deviated from the line of best fit near 0% and 100% filling fraction; therefore, we fit the data between approximately 30% and 70% filling fraction. To provide some guidance, we found that the intercepts approached a constant when $(w/10)(1-1/\epsilon_r) < h < (a-(w/10)(1-1/\epsilon_r))$ for $t < w$ by approximating the edge of the sample as a wire, computing when electric field decayed by a factor of 10.

From Fig. 5(a) and (b), we compared the measured real part of the permittivity with and without the holder, $\epsilon_r = 3.77 \pm 0.06$ (green with circles in online version) and $\epsilon_r = 3.78 \pm 0.06$ (blue with circles in online version). The corresponding loss tangents were $\tan\delta = 0.002 \pm 0.001$ (green in online version) and $\tan\delta = 0.000 \pm 0.001$ (blue in online version). Fig. 5(b) shows the real part of the complex permittivity as a function of filling fraction using the conventional technique and our approach. The extracted permittivity (ϵ_r) from the conventional technique described in [2] are shown for the quartz sample with (green solid in online version) and without the holder (blue solid in online version). Following the technique from [2], the real part of the permittivity was $\epsilon_r = 3.57$ at 100% filling fraction, which differs from the known result by about 6% [33]–[36]. In comparison, we plotted $\epsilon_r = (y_r + b_r)/2x$ in Fig. 5(b) as the green and blue lines with circles (in online version), which subtracted the effect of the intercepts. The thin black line is the permittivity (ϵ_r) obtained from the linear fit. The measured values for quartz obtained from the fit agreed with the known value to within 1%. The finite-element simulation results were consistent with the measured data on the quartz sample without the

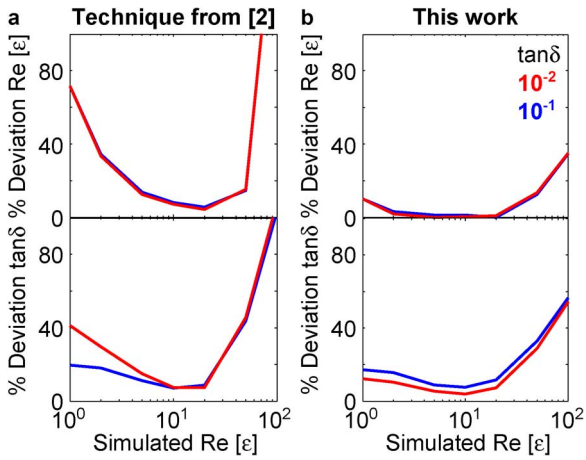

Fig. 6. Simulations of the percent deviations in ϵ and $\tan\delta$ from the finite-element simulation input parameters and those obtained from: (a) the conventional analysis method and (b) our method for our measurement setup. The simulated sample geometry is 3-mm wide and 0.5-mm thick. The red and blue curves (in online version) are for loss tangents $(\tan\delta)$ of 0.01 and 0.10, respectively.

holder for our measurement setup. Fig. 5(b) demonstrates that the effect of the nonuniform fields on the resonance frequency is nonlinear when the leading edge of the sample was near the sidewalls of the cavity and slot. Simulations near (but not at) 0% and 100% filling were inaccurate because the ratio of the largest to smallest feature size (feature aspect ratio) produced a computationally infeasible mesh. We could not simulate the sample holder because of the feature aspect ratio.

Next, we performed a series of finite-element simulations to test this technique for a range of permittivity and loss tangent values. In these simulations, we varied the height of the sample (h) from 3 to 7 mm in 1-mm steps. At each value of h, we then swept the loss tangent ($\tan\delta$ from 10^{-2} to 10^{-1}) and the real part of the complex permittivity (ϵ_r from 1 to 100) for our measurement setup. We performed the same simulations at 100% filling fraction to compute the deviation of the conventional technique. The simulation sample geometry was 3.0-mm wide (w), and 0.5-mm thick (t). We then calculated ω_o and ζ with the finite-element simulation. We computed the percent deviation of the technique in the real part of the permittivity as $100\cdot|(\epsilon_{\rm sim}-\epsilon_{\rm ext})|/\epsilon_{\rm sim}$ and in the loss tangent as $100\cdot|(\tan\delta_{\rm sim}-\tan\delta_{\rm ext})|/\tan\delta_{\rm sim}$. In Fig. 6, we compare the deviation of the conventional technique to our approach using the computed ω_o and ζ from over 100 finite-element simulations. From our analysis, the presented approach had a deviation in the real part of the permittivity of $\sim$1% for $2<\epsilon_r<20$. The deviation in the loss tangent for our technique was approximately 10% for $\epsilon_r<20$. Although these deviations were dependent on tested sample geometry and geometry of our cavity, we expect Fig. 6 to be representative for samples with similar geometries.

E. Step-by-Step Procedure

1) Configure resonant cavity.
2) Add a delay to unwrap the phase of the empty cavity or calibrate the VNA, depending on the measurement setup.
3) Affix the sample holder on the stage.
4) Define the zero position of the sample.
5) Measure complex S_{21} as a function of frequency for different filling fraction, following the $(w/10)(1-1/\epsilon_r)<h<(a-(w/10)(1-1/\epsilon_r))$ for $t<w$ guideline.
6) Place the sample on the sample holder and affix the sample holder onto the stage.
7) Measure complex S_{21} as a function of frequency for different filling fractions determined in Step 6.
8) Fit the data to a damped harmonic oscillator to obtain the natural frequency and the quality factor.
9) Correct the natural frequency and the quality factor for the holder.
10) Compute the relative frequency shift (y_r), the sample damping ratio (y_i), and the effective volume fraction (x).
11) Use a linear regression to fit the relative frequency shift (y_r) and the sample damping ratio (y_i) versus the effective volume fraction (x).
12) Extract the slopes to obtain the real and imaginary parts of the complex permittivity.

IV. Lossy Materials

In order to demonstrate this technique on lossy materials, we fabricated two freestanding films: a bisphenol A epoxy resin, and an MWCNT-epoxy nanocomposite (mass fraction of 3.5% MWCNT). The samples were processed from MWCNT supplied commercially as a mass fraction of 5% dispersed in the same liquid epoxy resin. The thicknesses (t) were (0.26 ± 0.02) mm and (0.30 ± 0.02) mm for samples with and without the carbon nanotubes. After the samples were cured, we used a dicing saw to cut the samples into strips, (5.04 ± 0.02) mm MWCNT-epoxy and (5.02 ± 0.02) mm epoxy. The samples were approximately 10-mm long. We used the same values for h as in the control experiments on quartz.

After we prepared the samples, we followed our measurement and correction procedure to obtain the relative frequency shift (y_r) and the sample damping ratio (y_i) as a function of filling fraction. In Fig. 7, we show the relative frequency shift (y_r) and the sample damping ratio (y_i) versus the effective volume fraction (x) in Fig. 7(a) and (c), respectively. The red line (in online version) is for the MWCNT-epoxy sample and the gray line is for the neat epoxy. Notice that the y-axis range of Fig. 7(c) is an order of magnitude larger than for the quartz sample in Fig. 4(a), hence it was much easier to quantify the losses of both samples as they were considerably larger than $1/Q$ of the cavity. Both samples show the positive deviation from the line of best fit at low and high percent filling fraction. In Fig. 6(b) and (d), we show the corresponding real and imaginary parts of the complex permittivity, respectively. The permittivity and loss tangent of the neat epoxy were $\epsilon_r=2.93\pm0.11$ and $\tan\delta=0.028\pm0.002$, respectively, and was consistent with previous reports near this frequency [37], [38]. The permittivity and loss tangent of the epoxy with a mass fraction of 3.5% MWCNTs were $\epsilon_r=8.01\pm0.48$ and $\tan\delta=0.137\pm0.010$, respectively. The conductivity $(\sigma=\omega\epsilon_o\epsilon_r\tan\delta)$ of the MWCNT epoxy was $\sim$ 0.5 S/m at 7.31 GHz and was consistent with a previous report [39].

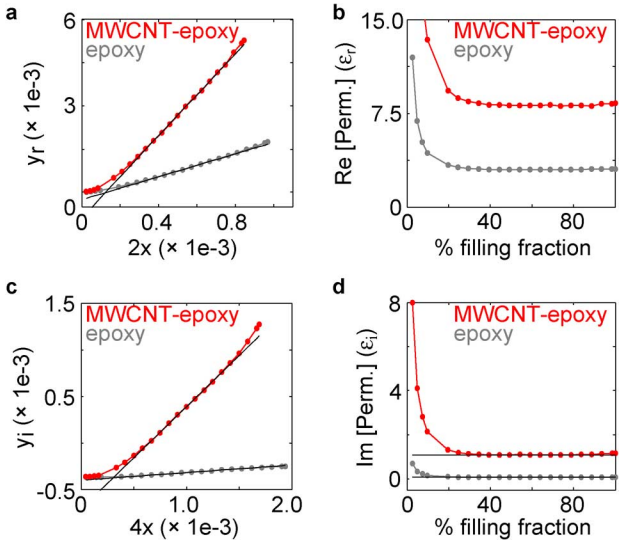

Fig. 7. Measurements of the relative frequency shift (y_r) in (a) and the sample damping ratio (y_i) in (c) versus the effective volume fraction (x) for the TE_{103} mode at approximately 7.31 GHz. In (b) and (d), we show the real and imaginary parts of the complex permittivity as a function of filling fraction. The red lines (in online version) were the results for the mass fraction 3.5% MWCNT-epoxy and the gray lines were for the neat epoxy.

V. Treatment of Uncertainty

In this section, we provide the analytical expressions for the uncertainty x, y_r, and y_i, which were used to obtain the complex permittivity from (8) and (9). The uncertainty for y_r and y_i were given by

$$|\Delta y_r|^2 = \left|\frac{\omega_s}{\omega_c^2}\right|^2 |\Delta\omega_c|^2 + \left|\frac{1}{\omega_c}\right|^2 |\Delta\omega_s|^2 \tag{14}$$

and

$$|\Delta y_i|^2 = \left|\frac{1}{Q_c^2}\right|^2 |\Delta Q_c|^2 + \left|\frac{1}{Q_s^2}\right|^2 |\Delta Q_s|^2 \tag{15}$$

respectively. Note that $\Delta\omega_c$ and ΔQ_c were obtained from the confidence interval in the fit, while $\Delta\omega_s$ and ΔQ_s were obtained from the error propagation of (10) and (11) in combination with the confidence interval. The uncertainty in x was given by

$$|\Delta x|^2 = \left|\frac{V_s'}{V_c^2}\right|^2 |\Delta V_c|^2 + \left|\frac{1}{V_c}\right|^2 |\Delta V_s'|^2 . \tag{16}$$

Next, we computed the uncertainty equations for the effective sample volume $(\Delta V_s')$ and volume of the cavity (ΔV_c). $\Delta V_s'$ accounts for the mode number (i.e., frequency). We then followed the fitting procedure outlined in [32], which properly treats the uncertainties in the fit. Although not as mathematically rigorous as [32], we decided to use the root-sum-of-squares (RSS) approach to approximate how each measurement variable contributed to the uncertainty in the complex permittivity. To do this, we solved (8) and (9) for the complex permittivity and then propagated the error. After computing the expressions analytically, we inserted (14)–(16) into our expressions for $\Delta\epsilon_r$ and $\Delta\epsilon_i$. We then used the measured values to compute the relative contributions to the uncertainty in the complex permittivity,

TABLE I
Error Contributions for the Quartz Sample

	Value	$\Delta\epsilon_r$	$\Delta\epsilon_i$
ΔV_c	50.7 mm^3	0.004	~0
ΔV_s	0.2 mm^3	0.086	~0
Δf_c	5.4 kHz	0.001	—
Δf_s	5.2 kHz	0.001	—
ΔQ_c	6.8	—	0.001
ΔQ_s	6.8	—	0.001
RSS error	—	0.09	0.002
[32] error	—	0.06	0.002

which we called the RSS error. In Table I, we show the approximate error contributions for the quartz sample. We noticed that the RSS method seemed to overestimate the errors compared to [32]. In more lossy samples, we found that the uncertainty in the sample volume dominated the uncertainty in the imaginary part of the permittivity. We found that the uncertainty increased with increasing mode number (n).

There were a few possible systematic errors that may have had varying impacts on the accuracy of this approach. Amongst these systematic errors, only the error in the absolute position of sample could have occurred here and not in conventional technique. We set the absolute position of the sample by bringing the leading edge of the sample in contact with a flat surface machined on the outside of the cavity. The resulting absolute position may deviate from the actual value by as much as 0.05 mm, which would affect both the intercept and slope. We determined that effect on the intercept and slope was less than respective uncertainties for our sample geometries and material properties. In practice, we found that minimum difference in the complex permittivity that we could detect is $\delta\tilde{\epsilon}/\tilde{\epsilon} \sim 2\%$, and would be significantly improved by more accurate measurement of the cavity and sample dimensions.

VI. Conclusions

In this paper, we have demonstrated several advances to the conventional microwave cavity perturbation technique. It has long been established that the sample interacting with the sidewalls and slot can adversely affect the accuracy of this technique. We have shown that by acquiring and fitting data over a range of filling fractions we were able to account for the resulting nonuniform fields, increasing the accuracy of this technique by about an order of magnitude for the sample properties and geometries measured here.

Within the regime where the contribution of the nonuniform field contributed as a nonzero intercept, we showed that the relative frequency shift and sample damping ratio were linearly dependent on the effective volume fraction. After we accounted for these fields, the resulting measurements on the quartz and bisphenol A samples were remarkably close to the accepted literature values. We applied this approach to a lossy MWCNT nanocomposite. Future work will examine the intercept as a function of complex permittivity. Finally, we developed an uncertainty analysis and concluded that the uncertainties in the dimensions of the sample geometry were the dominant source of error. To facilitate in the dissemination of this technique, we have published our analysis code in [40].

TABLE II
COMPARISON BETWEEN THE APPROACH WITH AND WITHOUT FITTING

	quartz	epoxy	MWCNT-epoxy
ϵ_r	3.78 ± 0.06	2.91 ± 0.11	8.01 ± 0.48
ϵ_i	$0.00 \pm 0.00(2)$	0.09 ± 0.01	1.16 ± 0.05
ϵ_r (without fitting)	3.83 ± 0.20	3.00 ± 0.48	7.89 ± 0.17
ϵ_i (without fitting)	0.14 ± 0.23	0.38 ± 0.48	1.35 ± 0.73

TABLE III
CIRCUIT PARAMETERS FOR TE_{103}

	cavity	holder	quartz	quartz+holder	
f_o[GHz]	7.32	7.29	7.30	7.27	
L_c[nH]	920	920	920	920	using [2]
C_c[fF]	0.5	0.5	0.5	0.5	
C_h[aF]	—	4.4	—	4.4	
C_s[aF]	—	—	2.6	2.6	
L[nH]	0.1	0.1	0.1	0.1	coupling
R[Ω]	0.04	0.04	0.04	0.04	
R_c[Ω]	15.1	15.1	15.1	15.1	cavity losses
G_h[nS]	—	2.9	—	2.9	dielectric losses
G_s[nS]	—	—	0.2	0.2	

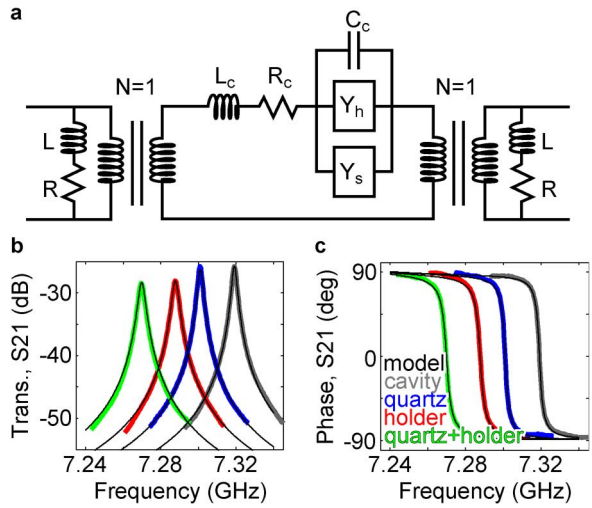

Fig. 8. (a) Lumped-element network model of our resonant cavity. Comparison between the measured and circuit simulations: (b) magnitude and (c) phase of the transmission. The gray, blue (in online version), red (in online version), and dark green (in online version) lines were for the cavity, cavity with the quartz, cavity with the holder, and the cavity with the sample on the holder. The thin black lines (simulated data) are the calculated S-parameters obtained by the circuit simulator using the parameters in Table III.

We summarize by stating that the ideal sample insertion is no longer simply a filling fraction of 100%. Rather, this technique is now only limited by the extent of the nonuniform fields in the sample and the magnitude of the perturbation.

APPENDIX A
SIMPLIFIED ANALYSIS

To facilitate streamlined measurements, we tested a simplified analysis procedure that does not require fitting the frequency dependence of complex S_{21} (see Table II). In the simplified case, we approximated the natural frequency as the peak frequency in S_{21}. We then approximated the quality factor with the 3-dB technique [25]. We then performed a linear regression [32] on the relative frequency shift (y_r) versus the effective volume fraction (x) to obtain the real part of the complex permittivity (see Section III). Although we obtained similar values, we found that fitting the data improved accuracy and decreased the uncertainty compared to the simplified technique. Table II shows the results for the TE_{103} mode at approximately 7.31 GHz.

APPENDIX B
RLC-CIRCUIT MODEL

Reference [2] provided an expression for the lumped-element capacitance and inductance that was used to model a single resonance frequency. In Table III, we show the natural frequencies and corresponding inductance and capacitance values for the cavity, the cavity with the holder, and the cavity with the quartz sample on the holder. We show the other lumped-element circuit parameters. All reported values were at 100% filling fraction for the TE_{103} mode.

We used electronic design automation software (or circuit simulator) to confirm that the capacitance added in parallel in order to validate our correction procedure. We first approximated the cross-coupling as two parallel sheets to estimate the coupling as an inductance of $L = (0.12 \pm 0.01)$ nH in series with a resistance of $R = (0.04 \pm 0.01)\ \Omega$. The model included the transmission lines with material properties taken from the specification sheet. We then tuned the series resistance of the cavity to match the measured quality factor in our measurement. We were able to reproduce our Q with a series resistance of $R_c = (15.12 \pm 0.01)\ \Omega$. Fig. 8(a) shows the equivalent network used to model the data. We then used circuit simulation software to obtain and the complex S-parameters using these parameters and the circuit model [see Fig. 8(a)]. In Fig. 8(a), we show the admittance element for the holder $(Y_h = G_h + i\omega C_h)$ and sample $(Y_s = G_s + i\omega C_s)$. We have listed the remaining circuit elements in Table III.

After we fit the Q of our measurements, we corrected the phase with an electrical delay in the simulation as we did in the measurement. These cavity and coupling parameters were held fixed for the other simulations. We then simulated the complex S-parameters as a function of frequency and added the parallel admittance for the holder, quartz, and quartz sample on the holder. In Fig. 8, we show the magnitude (b) and phase (c) of the transmission as a function of frequency for the cases shown in the Table III. We approximated the conductance as $G \approx \tan\delta \cdot \omega C$. For example, our initial estimate for the holder was computed as $G_h \approx (0.01) \cdot (2\pi \cdot 7.3\ \mathrm{GHz}) \cdot (4.4\ \mathrm{aF}) = 2.3$ nSQ. We tuned the conductance of the holder to fit the data found $G_h = (2.9 \pm 0.1)$ nS. This corresponded to a loss tangent that was slightly higher $(\tan\delta \approx 0.014)$ than our earlier measurements (Section III), but within the uncertainty. The conductance of the quartz in the model was 0.19 nS $(\tan\delta \approx 0.002)$. It is possible that this could be improved further to exactly reproduce the frequency dependence due to the losses, but our goal was only to validate that the admittances added in parallel.

APPENDIX C
CORRECTING FOR THE HOLDER

After we verified that the admittances added in parallel, we wanted to correct for the effect of the holder. In this case, we wrote the natural frequencies of the cavity (ω_c), cavity with the holder (ω_{ch}), and the cavity of the sample on the holder (ω_{chs}) as

$$\begin{aligned}\omega_c^{-2} &= LC_c \\ \omega_{ch}^{-2} &= L(C_c + C_h) \\ \omega_{chs}^{-2} &= L(C_c + C_h + C_s)\end{aligned}$$

where L was the inductance of the cavity, C_c was the capacitance of the cavity, C_h was the capacitance of the holder, and C_s was the capacitance of the sample. In the measurement, we obtained ω_c, ω_{ch}, and ω_{chs}, but require ω_{cs} (the natural frequency with the sample in the cavity without the holder). We then derived an expression to subtract the contribution of the holder off our measured data as

$$\omega_{cs}^{-2} = \omega_{chs}^{-2} - \omega_{ch}^{-2} + \omega_c^{-2} = L(C_c + C_s).$$

The quality factor of the cavity (Q_c), cavity with the holder (Q_{ch}), and the cavity of the sample on the holder (Q_{chs}) as

$$\begin{aligned}Q_c^{-1} &= Q_c^{-1} \\ Q_{ch}^{-1} &= Q_c^{-1} + Q_h^{-1} \\ Q_{chs}^{-1} &= Q_c^{-1} + Q_h^{-1} + Q_s^{-1}.\end{aligned}$$

We then combined these expressions to arrive at the quality factor of the cavity with the sample (Q_{cs})

$$Q_{cs}^{-1} = Q_{chs}^{-1} - Q_{ch}^{-1} + Q_c^{-1} = Q_c^{-1} + Q_s^{-1}.$$

This derivation is approximate because the port coupling could be dependent on the filling fraction.

ACKNOWLEDGMENT

The authors thank the critical review of Dr. J. McClelland, Dr. R. McMichael, Dr. M. Janezic, and Dr. T. M. Wallis, all with the National Institute of Standards and Technology (NIST), for their critical feedback during the course of this research, and their comments on this paper's manuscript. The authors thank Dr. T. Nguyen, NIST, for fabricating the samples. The authors also thank Dr. E. Rocas, Universitat Politecnica de Catalunya, for his insightful discussions regarding the lumped-element circuit modeling.

This paper is an official contribution of NIST; not subject to copyright in the US. Usage of commercial products herein is for information only; it does not imply recommendation or endorsement by NIST.

REFERENCES

[1] H. Bethe and J. Schwinger, "Perturbation theory for cavities," Cornell Univ., Ithaca, NY, USA, N.R.D.C. Tech. Rep. DI-117, Mar. 1943.

[2] C. G. Montgomery, R. H. Dicke, and E. M. Purcell, *Principles of Microwave Circuits*. Stevenage, U.K.: IET, 1948.

[3] H. B. G. Casimir, "On the theory of electromagentic waves in resonant cavities," Cornell Univ., Ithaca, NY, USA, Tech. Rep. 6, 1951.

[4] R. A. Waldron, "Perturbation theory of resonant cavities," *Proc. Inst. Elect. Eng.*, vol. 107, no. 12, pt. C, pp. 272–274, 1960.

[5] H. Bussey, "Measurement of RF properties of materials a survey," *Proc. IEEE*, vol. 55, no. 6, pp. 1046–1053, Jun. 1967.

[6] L. Chen, C. Ong, and B. T. G. Tan, "Amendment of cavity perturbation method for permittivity measurement of extremely low-loss dielectrics," *IEEE Trans. Instrum. Meas.*, vol. 48, no. 6, pp. 1031–1037, Jun. 1999.

[7] A. Parkash, J. K. Vaid, and A. Mansingh, "Measurement of dielectric parameters at microwave frequencies by cavity-perturbation technique," *IEEE Trans. Microw. Theory Techn.*, vol. MTT-27, no. 9, pp. 791–795, Sep. 1979.

[8] V. Subramanian, V. Sivasubramanian, V. R. K. Murthy, and J. Sobhanadri, "Measurement of complex dielectric permittivity of partially inserted samples in a cavity perturbation technique," *Rev. Sci. Instrum.* vol. 67, no. 1, p. 279, Jan. 1996. [Online]. Available: http://rsi.aip.org/resource/1/rsinak/v67/i1/p279_s1

[9] J. Baker-Jarvis, R. Geyer, J. Grosvenor, J. H. , M. Janezic, C. Jones, B. Riddle, C. Weil, and J. Krupka, "Dielectric characterization of low-loss materials a comparison of techniques," *IEEE Trans. Dielectr. Electr. Insul.*, vol. 5, no. 4, pp. 571–577, Aug. 1998.

[10] U. Kaatze, "Techniques for measuring the microwave dielectric properties of materials," *Metrologia*, vol. 47, no. 2, pp. S91–S113, Apr. 2010.

[11] P. Queffelec, V. Laur, A. Chevalier, J.-M. L. Floch, D. Passerieux, D. Cros, V. Madrangeas, A. L. Febvrier, S. Deputier, M. Guilloux-Viry, G. Houzet, T. Lacrevaz, C. Bermond, and B. Flechet, "Intercomparison of permittivity measurement techniques for ferroelectric thin layers," *J. Appl. Phys.* vol. 115, no. 2, Jan. 2014. [Online]. Available: http://scitation.aip.org/content/aip/journal/jap/115/2/10.1063/1.4858388, Art. ID 024103

[12] N. Orloff, J. Mateu, M. Murakami, I. Takeuchi, and J. C. Booth, "Broadband characterization of multilayer dielectric thin-films," in *IEEE MTT-S Int. Microw. Symp. Dig.*, 2007, vol. 1–6, pp. 1174–1177.

[13] C.-H. Lee, N. D. Orloff, T. Birol, Y. Zhu, V. Goian, E. Rocas, R. Haislmaier, E. Vlahos, J. A. Mundy, L. F. Kourkoutis, Y. Nie, M. D. Biegalski, J. Zhang, M. Bernhagen, N. A. Benedek, Y. Kim, J. D. Brock, R. Uecker, X. X. Xi, V. Gopalan, D. Nuzhnyy, S. Kamba, D. A. Muller, I. Takeuchi, J. C. Booth, C. J. Fennie, and D. G. Schlom, "Exploiting dimensionality and defect mitigation to create tunable microwave dielectrics," *Nature* vol. 502, no. 7472, pp. 532–536, Oct. 2013. [Online]. Available: http://www.nature.com/nature/journal/v502/n7472/abs/nature12582.html

[14] B. Meng, J. Booske, and R. Cooper, "Extended cavity perturbation technique to determine the complex permittivity of dielectric materials," *IEEE Trans. Microw. Theory Techn.*, vol. 43, no. 11, pp. 2633–2636, Nov. 1995.

[15] H. Kobayashi and S. Ogawa, "Dielectric constant and conductivity measurement of powder samples by the cavity perturbation method," *Jpn. J. Appl. Phys.* vol. 10, no. 3, pp. 345–350, 1971. [Online]. Available: http://jjap.jsap.jp/link?JJAP/10/345/

[16] A. Verma and D. C. Dube, "Measurement of dielectric parameters of small samples at X-band frequencies by cavity perturbation technique," *IEEE Trans. Instrum. Meas.*, vol. 54, no. 5, pp. 2120–2123, Oct. 2005.

[17] C. P. L. Rubinger and L. C. Costa, "Building a resonant cavity for the measurement of microwave dielectric permittivity of high loss materials," *Microw. Opt. Technol. Lett.* vol. 49, no. 7, pp. 1687–1690, 2007. [Online]. Available: http://onlinelibrary.wiley.com/doi/10.1002/mop.22506/abstract

[18] M. D. Janezic and J. Baker-Jarvis, "Full-wave analysis of a split-cylinder resonator for nondestructive permittivity measurements," *IEEE Trans. Microw. Theory Techn.*, vol. 47, no. 10, pp. 2014–2020, Oct. 1999.

[19] M. Janezic, E. F. Kuester, and J. Jarvis, "Broadband complex permittivity measurements of dielectric substrates using a split-cylinder resonator," in *IEEE MTT-S Int. Microw. Symp. Dig.*, Jun. 2004, vol. 3, pp. 1817–1820.

[20] M. Lin, Y. Wang, and M. Afsar, "Precision measurement of complex permittivity and permeability by microwave cavity perturbation technique," in *Joint 30th Int. Infrared Millim. Waves Conf./13th Int. Terahertz Electron. Conf.*, 2005, vol. 1, pp. 62–63.

[21] V. Murthy and R. Raman, "A method for the evaluation of microwave dielectric and magnetic parameters using rectangular cavity perturbation technique," *Solid State Commun.* vol. 70, no. 8, pp. 847–850, May 1989. [Online]. Available: http://www.sciencedirect.com/science/article/pii/0038109889905103
[22] D. Higginbottom, M. Howes, and J. Richardson, "An experimental technique to evaluate the complex permittivity of small samples of microwave substrates," in *16th Eur. Microw. Conf.*, 1986, pp. 790–795.
[23] R. Thomas and D. C. Dube, "Extended technique for complex permittivity measurement of dielectric films in the microwave region," *Electron. Lett.*, vol. 33, no. 3, pp. 218–220, Jan. 1997.
[24] K. Sudheendran, D. Pamu, M. G. Krishna, and K. C. J. Raju, "Determination of dielectric constant and loss of high-k thin films in the microwave frequencies," *Measurement*, vol. 43, no. 4, pp. 556–562, May 2010.
[25] P. J. Petersan and S. M. Anlage, "Measurement of resonant frequency and quality factor of microwave resonators: Comparison of methods," *J. Appl. Phys.*, vol. 84, no. 6, pp. 3392–3402, Sep. 1998.
[26] B. Nebendahl, D. N. Peligrad, M. Pozek, A. Dulcic, and M. Mehring, "An AC method for the precise measurement of Q-factor and resonance frequency of a microwave cavity," *Rev. Sci. Instrum.*, vol. 72, no. 3, pp. 1876–1881, Mar. 2001.
[27] K. J. Coakley, J. D. Splett, M. D. Janezic, and R. F. Kaiser, "Estimation of q-factors and resonant frequencies," *IEEE Trans. Microw. Theory Techn.*, vol. 51, no. 3, pp. 862–868, Mar. 2003.
[28] D. Sorensen, "Newton's method with a model trust region modification," *SIAM J. Numer. Anal.* vol. 19, no. 2, pp. 409–426, Apr. 1982. [Online]. Available: http://epubs.siam.org/doi/abs/10.1137/0719026
[29] D. Kajfez, "Correction for measured resonant frequency of unloaded cavity," *Electron. Lett.*, vol. 20, no. 2, pp. 81–82, Jan. 1984.
[30] K. Leong and J. Mazierska, "Precise measurements of the q factor of dielectric resonators in the transmission mode-accounting for noise, crosstalk, delay of uncalibrated lines, coupling loss, and coupling reactance," *IEEE Trans. Microw. Theory Techn.*, vol. 50, no. 9, pp. 2115–2127, Sep. 2002.
[31] A. Canos, J. Catala-Civera, F. Penaranda-Foix, and E. Reyes-Davo, "A novel technique for deembedding the unloaded resonance frequency from measurements of microwave cavities," *IEEE Trans. Microw. Theory Techn.*, vol. 54, no. 8, pp. 3407–3416, Aug. 2006.
[32] D. York, N. M. Evensen, M. L. Martinez, and J. D. Delgado, "Unified equations for the slope, intercept, and standard errors of the best straight line," *Amer. J. Phys.*, vol. 72, no. 3, pp. 367–375, Mar. 2004.
[33] D. M. Pozar, "Considerations for millimeter wave printed antennas," *IEEE Trans. Antennas Propag.*, vol. AP-31, no. 5, pp. 740–747, May 1983.
[34] V. Varadan, R. Hollinger, D. Ghodgaonkar, and V. Varadan, "Free-space, broadband measurements of high-temperature, complex dielectric-properties at microwave-frequencies," *IEEE Trans. Instrum. Meas.*, vol. 40, no. 5, pp. 842–846, Oct. 1991.
[35] Y. G. Makeev and A. P. Motornenko, "Measuring the electric parameters of dielectrics at microwave frequencies," *Instrum. Experiment. Techn.* vol. 46, no. 1, pp. 60–64, Jan. 2003. [Online]. Available: http://link.springer.com/article/10.1023/A
[36] E. Li, Z. Nie, G. Guo, Q. Zhang, Z. Li, and F. He, "Broadband measurements of dielectric properties of low-loss materials at high temperatures using circular cavity method," *Progr. Electromagn. Res.*, vol. 92, pp. 103–120, 2009.
[37] C. Hsuan Lin, J. Chung Chiang, and C. Shan Wang, "Low dielectric thermoset. I. Synthesis and properties of novel 2,6-dimethyl phenol-dicyclopentadiene epoxy," *J. Appl. Polymer Sci.* vol. 88, no. 11, pp. 2607–2613, 2003. [Online]. Available: http://onlinelibrary.wiley.com/doi/10.1002/app.11874/abstract
[38] S. Singha and M. Thomas, "Permittivity and tan delta characteristics of epoxy nanocomposites in the frequency range of 1 MHz–1 GHz," *IEEE Trans. Dielectr. Electr. Insul.*, vol. 15, no. 1, pp. 2–11, Feb. 2008.
[39] A. Allaoui, S. Bai, H. Cheng, and J. Bai, "Mechanical and electrical properties of a MWNT/epoxy composite," *Composites Sci. Technol.* vol. 62, no. 15, pp. 1993–1998, Nov. 2002. [Online]. Available: http://www.sciencedirect.com/science/article/pii/S026635380200129X
[40] N. D. Orloff, "Dielectric characterization by microwave cavity perturbation," *File Exchange—MATLAB Central* [Online]. Available: http://www.mathworks.com/matlabcentral/fileexchange/file_infos/46537-dielectric-characterization-by-microwave-cavity-perturbation [accessed: 07 May 2014]

Nathan D. Orloff received the B.S. degree in physics (with high honors) and Ph.D. degree in physics from the University of Maryland at College Park, College Park, MD, USA, in 2004 and 2010, respectively. His doctoral thesis concerned the study and extraction of microwave properties of ferroelectrics.

In 2011, he was a Dean's Postdoctoral Fellow with the Department of Bioengineering, Stanford University. In 2013, he joined the Materials Measurement Laboratory, National Institute of Standards and Technology (NIST), Gaithersburg, MD, USA, as a Rice University Postdoctoral Fellow.

Dr. Orloff was the recipient of the 2004 Martin Monroe Undergraduate Research Award, the 2006 CMPS Award for Excellence as a Teaching Assistant, and the 2010 Michael J. Pelczar Award for Excellence in Graduate Study.

Jan Obrzut received the Ph.D. degree in technical sciences from the Institute of Physics, Cracov Polytechnic, Poland, in 1981.

After a postdoctoral appointment with the Polymer Science Department, University of Massachusetts, he was a Researcher with the Five College Radio Astronomy Department, Amherst, MA, USA, where he was involved with microwave dielectric waveguides. In 1988, he joined IBM, as an Advisory Engineer, where he conducted exploratory work on application of polymer dielectrics in microelectronics. Since 1997, he has been with the NIST Polymers, Gaithersburg, MD, USA, where he researches dielectric films and hybrid materials for microwave and electronic applications. His research interests include embedded passive devices and nano-carbon electronic materials.

Christian J. Long received the B.S. and Ph.D. degrees in physics from the University of Maryland at College Park, College Park, MD, USA. His doctoral research focused on the development of novel microwave near-field scanning probe microscopy techniques and on the development of new methods to analyze data from combinatorial materials experiments.

He is currently a CNST/UMD Postdoctoral Researcher with NIST, where he is involved with characterize friction on the nanometer length scale by a combination of atomic force microscopy and Raman spectroscopy.

Thomas Lam received the B.S. and M.S. degrees in ceramic engineering and the Ph.D. degree in ceramics from Alfred University, Alfred, NY, USA. His doctoral research applied glass formation theory to explain grain boundary evolution in the sintering of alumina.

During his doctoral studies, he was with the Department of Energy National Energy Technology Laboratory (NETL), where he studied skutterudite material, gasifier refractories, and mixtures of synthetic coal and petcoke slags. He is currently a Postdoctoral Researcher with the Center for Nanoscale Science and Technology, National Institute of Standards and Technology (NIST), Gaithersburg, MD, USA.

Dr. Lam was the recipient of the 2012 American Ceramic Society Richard and Patricia Spriggs Phase Equilibria Award.

Pavel Kabos (SM'93–F'05) received the Ph.D. and M.S. degrees in solid-state physics from the Slovak University of Technology, Bratislava, Slovakia, where he joined the Faculty of Electrical Engineering and Information Technology, Department of Electromagnetic Theory, in 1972. From 1982 to 1984, he was a Postdoctoral Fellow with the Department of Physics, Colorado State University, continuing as a Visiting Scientist and a Research Professor in 1991. In 1998, he joined the National Institute of Standards and Technology (NIST), Boulder, CO, USA, and in 2001, became a Staff Physicist with the Electromagnetics Division, NIST. He has authored or coauthored over 110 archival papers, several book chapters, and a book. His research concerns linear and nonlinear precession dynamics, metrology for high-speed nanoelectronics, scanning probe microscopy, dielectric and magnetic materials spectroscopy, nondestructive electromagnetic evaluation, and numerical methods for electromagnetic field analysis.

Dr. Kabos is currently the editor-in-chief of the IEEE TRANSACTIONS ON MAGNETICS.

David R. Novotny received the B.S.E.E. and M.S.E.E. degrees from the University of Colorado at Boulder, Boulder, CO, USA. His graduate work focused on the design of specialized nonperturbing dielectric mounts for antennas.

He is currently with the Physical Measurement Laboratory, National Institute of Standards and Technology (NIST), Boulder, CO, USA, where his major research topics include electromagnetic (EM) material evaluation, RF identification (RFID), antenna design and calibration, and millimeter-wave and terahertz measurement systems.

Dr. Novotny was the recipient of the Department of Commerce Gold Medal for his work on the characterization and improvement of security of the US ePassport, a Bronze Medal for analysis of the US Western Hemisphere Travel Card, and a Bronze Medal for EM shielding evaluation of the Space Shuttle Orbiter.

James C. Booth received the B.A. degree in physics from the University of Virginia, Charlottesville, VA, USA, in 1989 and the Ph.D. degree in physics from the University of Maryland at College Park, College Park, MD, USA, in 1996. His dissertation concerned novel measurements of the frequency dependent microwave surface impedance of cuprate thin-film superconductors.

Since 1996, he has been a Physicist with the National Institute of Standards and Technology (NIST), Boulder, CO, USA, where he was previously a National Research Council (NRC) Postdoctoral Research Associate (1996–1998). He is currently the leader of the High Frequency Devices and Characteristics Project. His research at NIST is focused on exploring the microwave properties of new electronic materials and devices, including ferroelectric, magneto-electric, and superconducting thin films, as well as developing experimental platforms integrating microfluidic and microelectronic components for RF and microwave-frequency characterization of liquid and biological samples.

J. Alexander Liddle received the B.A. and D. Phil. degrees in materials science from the University of Oxford, Oxford, U.K., in 1986 and 1989, respectively.

He spent the next 11 years with Bell Laboratories, where his primary efforts were directed toward the research, development, and eventual commercialization of a novel electron-beam lithography technology. He spent the next three years as the Head of the LBNL Nanofabrication Group, Center for X-Ray Optics, prior to becoming Lead Scientist of the Molecular Foundry Nanofabrication User Facility, where he was involved in research ranging from quantum computation to guided self-assembly. In 2006, he joined the National Institute of Standards and Technology (NIST), Gaithersburg, MD, USA, where he is the Leader of the Nanofabrication Research Group, Center for Nanoscale Science and Technology. He has authored or coauthored over 200 papers. His current research focus is on nanofabrication and self-assembly for nanomanufacturing.

Dr. Liddle is a Fellow of the APS.